Supporting information

Synchronizing Proton-Electron Transfer in Nanoconfined Cu-Ni Alloys Enables Highly Selective Nitrate-to-Ammonia Conversion

*Puxia Yan, Zichao Huang, Yingbing Zhang, Lin Gu, Suxin Bai, Yulu Hua, Min Kuang *, and Jianping Yang**

State Key Laboratory of Advanced Fiber Materials, College of Materials Science and Engineering, Donghua University, Shanghai 201620, China

Experimental Section

Materials and chemicals

Copper(II) acetate ($C_4H_6CuO_4$, 98%) was purchased from Shanghai Bide Pharmatech Co., Ltd. Nickel(II) acetate tetrahydrate ($C_4H_{14}NiO_8$, 99%) was obtained from Innochem. N,N-Dimethylformamide (DMF, C_3H_7NO, 99%) was supplied by Shanghai Titan Technology Co., Ltd. Polyacrylonitrile ($(C_3H_3N)_x$, average M.W. 150,000) was acquired from Shanghai Macklin Biochemical Co., Ltd. Poly(methyl methacrylate) (PMMA, $(C_5H_8O_2)_x$) was obtained from Sinopharm Chemical Reagent Co., Ltd. Potassium hydroxide (KOH, 95%) was purchased from Shanghai Macklin Biochemical Co., Ltd. Potassium nitrate (KNO_3, AR grade) was obtained from Sinopharm Chemical Reagent Co., Ltd. Sodium hydroxide (NaOH, AR grade) was purchased from Sinopharm Chemical Reagent Co., Ltd. Salicylic acid ($C_6H_4(OH)COOH$, 99.5%) was obtained from Rhawn Chemical Technology Co., Ltd. Sodium citrate dihydrate ($Na_3C_6H_5O_7·2H_2O$, 99%) was supplied by Shanghai Aladdin Biochemical Technology Co., Ltd. Sodium nitroprusside dihydrate ($Na_2[Fe(CN)_5NO]·2H_2O$, 99%) was purchased from Shanghai Macklin Biochemical Technology Co., Ltd. Sodium hypochlorite solution (available chlorine ≥5%) was obtained from Shanghai Aladdin Biochemical Technology Co., Ltd. Sulfuric acid (H_2SO_4, 95-98%) and ammonium chloride (NH_4Cl, 99.5%) were both purchased from Sinopharm Chemical Reagent Co., Ltd. Isopropanol (C_3H_8O, 99%) was obtained from Beijing Creative Chemical Technology Co., Ltd. Nafion solution (5 wt.%) in a mixture of lower aliphatic alcohols and water) was procured from Sigma-Aldrich. Hydrophilic carbon paper was supplied by Kunshan Development Zone Kaiweiyue Electronic Trading Department. The DuPont proton exchange membrane was acquired from Kunshan Development Zone Kaiminke Trading Firm. All chemicals and materials were used as received without further purification.

Characterizations

The Cu_2Ni-CNF composite was prepared via an electrospinning method. Copper(II) acetate and nickel(II) acetate were first dissolved in 5 mL of DMF under magnetic stirring for 10 minutes to form a homogeneous solution, with the molar ratio of Cu to Ni varying from 1:0 to 0:1. Subsequently, 375 mg of PAN and 150 mg of PMMA (mass ratio of 2.5:1) were added to the solution, followed by continuous magnetic stirring for 720 minutes to obtain a homogeneous and viscous spinning precursor. The precursor solution was then loaded into a syringe for electrospinning. Under a high voltage of 18-20 kV, the solution was extruded at a flow rate of 0.5 ML/h, overcoming surface tension to form solidified fibrous filaments. The collected fibers were wound onto a rotating drum at 200 rpm, with a lateral traverse speed of 20 mm/s. During this process, copper/nickel species and PMMA particles were effectively incorporated into or

onto the fiber matrix. The as-spun fibers were subsequently subjected to thermal treat ments. First, they were dried at 60 °C for 12 hours under air flow to stabilize the fib rous morphology. Then, the dried sample was calcined in a muffle furnace at 220 °C for 2 hours under air. Finally, the calcined product was transferred to a tube furnace and reduced at 600 °C (heating rate: 5 °C/min) under a 5 vol% H_2/Ar atmosphere for 120 minutes. After reduction, the system was cooled naturally to room temperature un der the same gas flow.

Materials Characterization

X-ray diffraction (XRD) patterns were recorded on a MiniFlex600-C diffractometer equipped with Cu Kα radiation. The microstructure and elemental distribution of the samples were characterized using scanning electron microscopy (SEM, Regulus8230), transmission electron microscopy (TEM, Talos F200S), high-angle annular dark-field scanning TEM (HAADF-STEM, JEM-2100F), and energy-dispersive X-ray spectroscopy (EDX) elemental mapping. Nitrogen adsorption-desorption isotherms were measured at 77 K using an Autosorb IQ automated gas adsorption analyzer. The specific surface area was calculated using the Brunauer-Emmett-Teller (BET) method, while the pore volume and pore size distribution were derived from the Barrett-Joyner-Halenda (BJH) model. In-situ attenuated total reflectance Fourier-transform infrared (ATR-FTIR) spectra were collected using a Spectrum 3 spectrometer (PerkinElmer, USA). The metal content in the samples and the composition of the post-reaction electrolyte were quantitatively analyzed by inductively coupled plasma optical emission spectrometry (ICP-OES). The chemical states of elements in the electrocatalysts were investigated by X-ray photoelectron spectroscopy (XPS) on an Escalab 250Xi system using Al Kα radiation as the excitation source. Differential electrochemical mass spectrometry (DEMS) measurements were conducted on a Linglu QAS 100 system to enable real-time analysis of reaction intermediates and products. Raman spectra were acquired on a inVia-Reflex spectrometer using a 532 nm laser excitation to probe the defect structures of the materials.

Electrocatalytic performance measurements

All electrochemical tests were performed at room temperature and atmospheric pressure using a conventional three-electrode system on a CS310X multichannel electrochemical workstation. An H-type electrolytic cell was employed, with a saturated calomel electrode (SCE) as the reference electrode and a platinum foil (surface area: 1 cm^2) as the counter electrode. The working electrode was fabricated by drop-casting catalyst ink onto hydrophilic carbon paper. Working Electrode Preparation, 5 mg of the catalyst was ultrasonically dispersed in a mixture containing 0.23 mL of deionized water (resistivity 18.20 MΩ • cm), 0.72 mL of isopropanol (analytical grade), and 50 uL of Nafion solution (5 wt.%). The resulting catalyst ink was uniformly deposited onto the hydrophilic carbon paper (coating area: 1 cm^2) and dried under an infrared lamp. Each compartment of the H-cell was filled with 25 mL of electrolyte

that had been pre-purged with argon for 30 min to remove dissolved oxygen. The cathode chamber contained a 1 M KOH/0.1 M KNO_3 solution, while the anode chamber was filled with 1 M KOH. Prior to each test, the catalyst was activated by chronoamperometry (CA) to stabilize the system. The activation was performed by sweeping the potential from -1.7 V to -1.4 V (vs. SCE) at 10 mV/s, holding each potential for 0.5 h. Linear sweep voltammetry (LSV) was then conducted from -2 V to 0 V (vs. SCE) at 10 mV/s to evaluate the electrocatalytic activity of the cathode for the nitrate reduction reaction (NO_3RR) in the presence and absence of KNO_3. Subsequent chronoamperometric tests were carried out at various constant potentials ranging from -1.7 V to -1.1 V (vs. SCE), with each potential held for 1 h. The reaction products were quantified using ultraviolet-visible spectrophotometry to determine the Faradaic efficiency and yield of ammonia production. Throughout the measurements, the electrolyte was stirred at 500 rpm. Electrochemical impedance spectroscopy (EIS) was performed in the frequency range of 0.1 Hz to 1 MHz. The electrochemical active surface area (ECSA) was estimated from the electrochemical double-layer capacitance (C_{dl}). Cyclic voltammetry (CV) was scanned within a non-Faradaic potential window at sweep rates of 40, 60, 80, 100, and 120 mV/s. The linear slope of the current density versus scan rate plot at a given potential corresponds to C_{dl}, which is proportional to the ECSA. No *iR* compensation was applied to any electrochemical data reported in this work.

Long-cycle performance test

For long-term cycling performance testing, chronoamperometry was conducted at a constant potential of -0.5 V (vs. RHE) using Cu_2Ni-CNF as the working electrode, a saturated calomel electrode (SCE) as the reference electrode, and a platinum foil with a surface area of 1 cm^2 as the counter electrode. Each compartment of the H-cell was filled with 25 mL of electrolyte, where the cathode chamber contained a 1 M KOH/0.1 M KNO_3 solution, and the anode chamber was filled with 1 M KOH. Each test cycle lasted for one hour, after which a small aliquot of electrolyte was sampled. The ammonia concentration in the electrolyte was quantified using ultraviolet-visible spectrophotometry to analyze the Faradaic efficiency and production yield of the nitrate reduction reaction.

UV-vis analysis for ionic concentration determination in solution

The ammonia concentration was determined using the indophenol blue spectrophotometric method with a Thermo Fischer Scientific Evolution 200 UV-Vis spectrophotometer. The colorimetric reagent was prepared from a 5% salicylic acid solution, a 1% sodium nitroferricyanide solution, and a 0.05 $mol \cdot L^{-1}$ sodium hypochlorite solution. For each measurement, 0.05 mL of the electrolyte sample was added to a 25 mL colorimetric tube, followed by 23.2 mL of 0.005 $mol \cdot L^{-1}$ H_2SO_4, 1.25 mL of 5% salicylic acid, 0.25 mL of 1% sodium nitroferricyanide, and 0.25 mL of 0.05 $mol \cdot L^{-1}$ sodium hypochlorite. The mixture was thoroughly stirred and then allowed to stand at room temperature for 1 h. The absorbance of the

resulting solution was measured at 697 nm using a 5 mm path-length cuvette with deionized water as the reference. A calibration curve was established using a series of standard ammonium chloride (or ammonium sulfate) solutions to ensure accurate quantification.

All measured potentials were converted to the reversible hydrogen electrode (RHE) scale using the following equation:

$$E_{RHE} = E_{Ho/HoO} + 0.244 + 0.0591 \times (pH) \quad (S1)$$

The NH_3 concentration (CNH_3) was determined using a calibration curve derived from standard ammonia solutions. The ammonia production rate was subsequently calculated according to Equation (S2)：

$$NH_3 yield = \frac{C_{NH_3} \times V}{t \times A} \quad (S2)$$

The Faradaic efficiency (FE) for NH_3 production was calculated using Equation (S3)：

$$NH_3 FE = \frac{8 \times F \times C_{NH_3} \times V}{17 \times Q} \quad (S3)$$

here: V represents the volume of the catholyte in milliliters (mL); CNH_3 represents the concentration of ammonia (M); t is the electrolysis time; A represents absorbance; F is the Faraday constant (96485 $C \cdot mol^{-1}$); Q represents the number of electrons transferred.

In situ DEMS analysis

The differential electrochemical mass spectrometry (DEMS, QAS 100) was provided by Linglu Instrument (Shanghai) Co. Ltd. DEMS. To identify the intermediates and products generated during nitrate reduction to ammonia, differential electrochemical mass spectrometry (DEMS) measurements were performed. Prior to analysis, a stable baseline was established. The electrolyte used was 0.1 M KNO_3, and measurements were conducted in a three-electrode configuration, where the catalyst served as the working electrode, a platinum wire as the counter electrode, and a Hg/HgO electrode as the reference electrode. Chronoamperometry (CA) was then carried out by stepping the potential to -1.3 V (vs. SCE) at a scan rate of 10 mV/s, with each potential held for 30 s. The gaseous and volatile species generated during electrolysis were continuously transported via a capillary inlet into the mass spectrometer for real-time analysis. After each test, the system was allowed to return to the baseline signal level before proceeding to the next measurement. To ensure data accuracy and reproducibility, three independent CA tests were performed under identical conditions.

In situ ATR-FTIR spectrometry

In-situ electrochemical attenuated total reflection Fourier-transform infrared (ATR-FTIR) spectroscopy was performed using a custom-designed Spectro electrochemical cell (Shanghai Yuanfang Technology Co., Ltd.) coupled with a CHI660 electrochemical workstation. Spectra were recorded on a Thermo Nicolet Nexus 670 spectrometer. The absorbance of the sample was monitored under working conditions. In the resulting differential absorption spectra, positive bands indicate the formation of products or intermediates, while negative bands correspond to the consumption of reactants or the breaking of chemical bonds. The measurements were conducted in a 1 M KOH/0.1 M KNO_3 electrolyte. A background spectrum was first collected at the open-circuit potential. Subsequently, chronoamperometric tests were performed by stepping the potential from lower to higher values, with each potential held for 60 s. Infrared signals were collected in the range of 1000-4000 cm^{-1}.

Assemble Zn-NO_3^- battery

The Zn-NO_3^- battery was assembled using Cu_2Ni-CNF as the cathode and a zinc plate as the anode. A conventional H-type cell was employed, containing 25 mL of catholyte (1 M KOH + 0.1 M KNO_3) and 25 mL of anolyte (1 M KOH), separated by a bipolar membrane. Discharge polarization curves were recorded on a CHI660 electrochemical workstation at a scan rate of 5 Mv/s, followed by galvanostatic discharge tests. After the electrochemical measurements, the electrolyte was diluted to an appropriate concentration, and the ammonia concentration was quantified by ultraviolet-visible spectrophotometry. The electrochemical reaction at the cathode of the Zn-NO_3^- battery is as follows $NO_3^- + 7H_2O + 8e^- \rightarrow NH_4OH + 9OH^-$. The anodic reaction is: $4Zn + 8OH^- \rightarrow 4ZnO + 4H_2O + 8e^-$. The overall cell reaction is: $4Zn + NO_3^- + 3H_2O \rightarrow 4ZnO + NH_4OH + OH^-$.

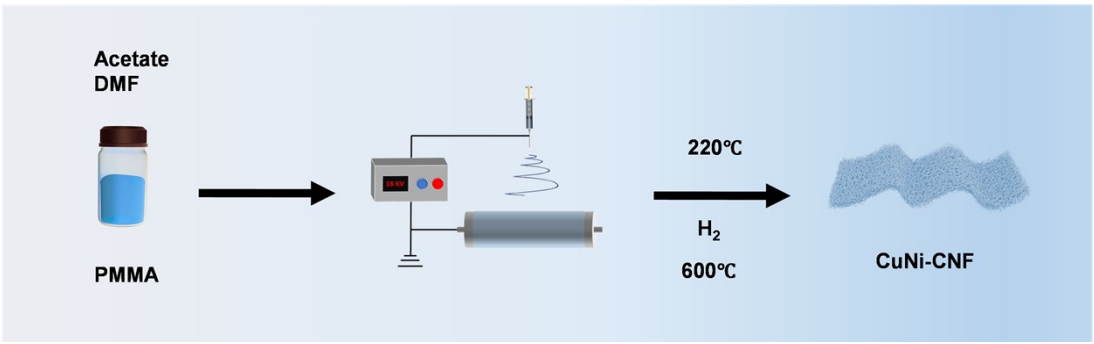

Fig. S1 Schematic diagram of the preparation of Cu-Ni alloy catalyst by electrospinning followed by heat treatment.

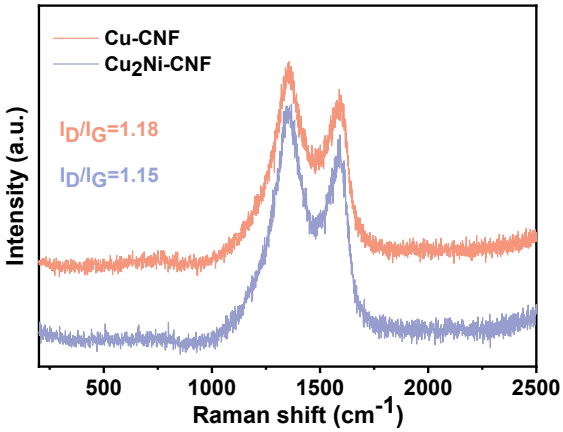

Fig. S2 Raman spectra of Cu-Ni alloy catalyst.

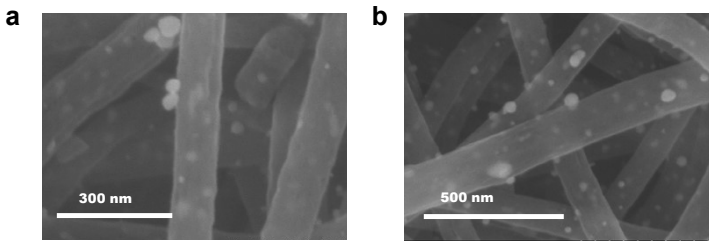

Fig. S3 SEM images of Cu-Ni alloy catalyst a) the Cu-CNF catalyst. b) the Cu_2Ni-CNF catalyst.

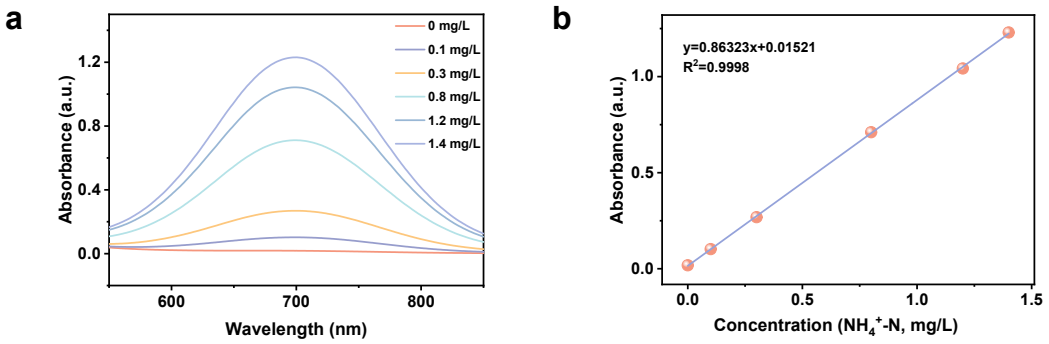

Fig. S4 UV-vis spectroscopic calibration for ammonium ion determination. a) UV-vis absorption spectra of standard NH_4^+ solutions. The absorbance at the characteristic wavelength of 697 nm (indicated by the dashed line) was used for quantification. b) Linear calibration curve derived from the absorbance at 697 nm, with the regression equation and R^2 value displayed.

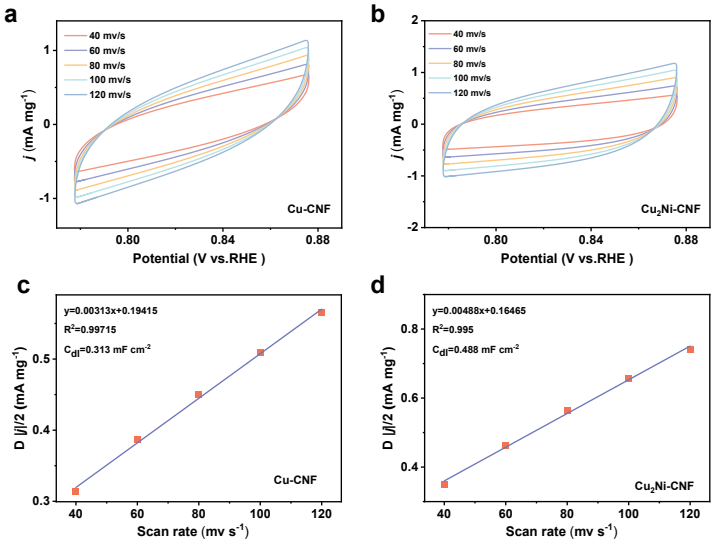

Fig. S5 a-b) Cyclic voltammograms of Cu-Ni alloy catalyst. c-d) Capacitive current densities at 0.827 V (vs. RHE) derived from CVs of Cu-Ni alloy catalyst.

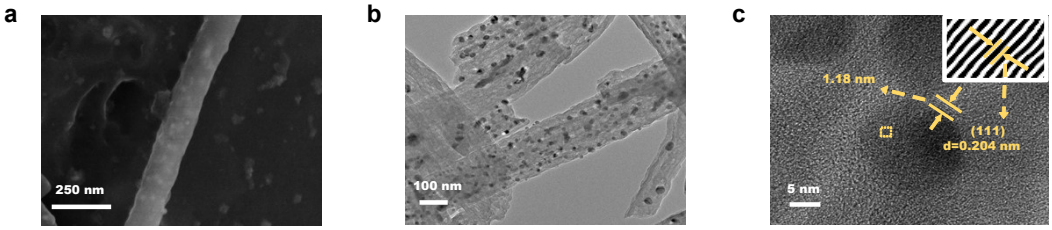

Fig. S6 a) SEM image of Cu_2Ni-CNF catalyst after chronoamperometry (0.1 M KOH + 0.1 M KNO_3). b-c) TEM images at different magnifications of the Cu_2Ni-CNF catalyst after chronoamperometry at -0.7 V (vs. RHE) in NO_3^--containing electrolyte (0.1 M KOH + 0.1 M KNO_3).

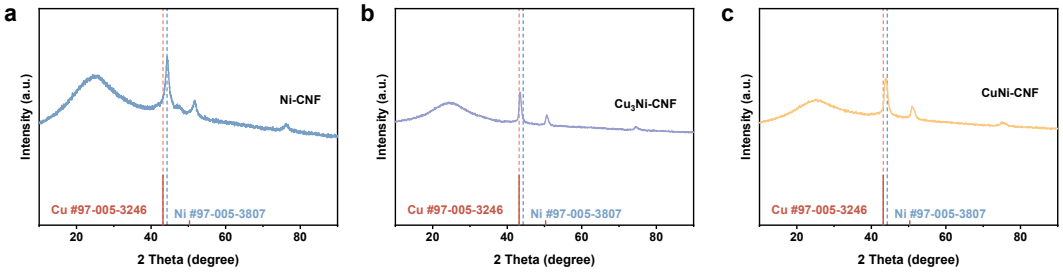

Fig. S7 a-c) XRD patterns of Cu-Ni alloy catalyst.

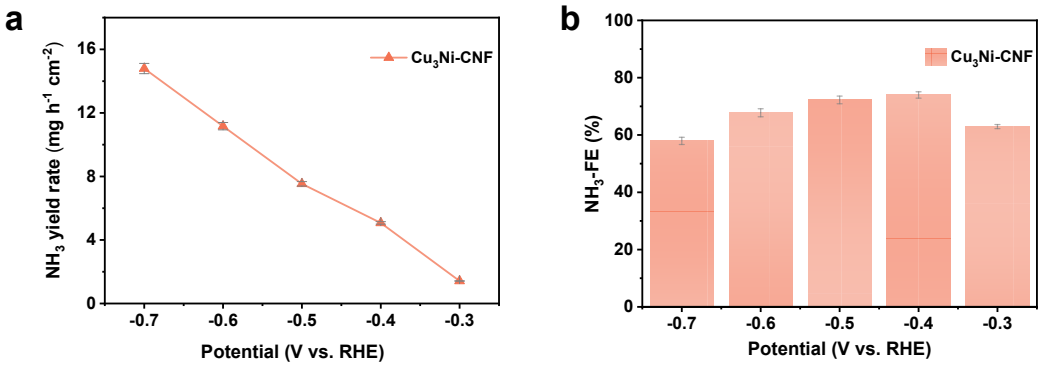

Fig. S8 a) The products formation rate of Cu_3Ni-CNF catalyst measured after 1 hour of chronoamperometry at different potential. b) Faraday efficiency of Cu_3Ni-CNF catalyst measured after 1 hour of chronoamperometry at different potential.

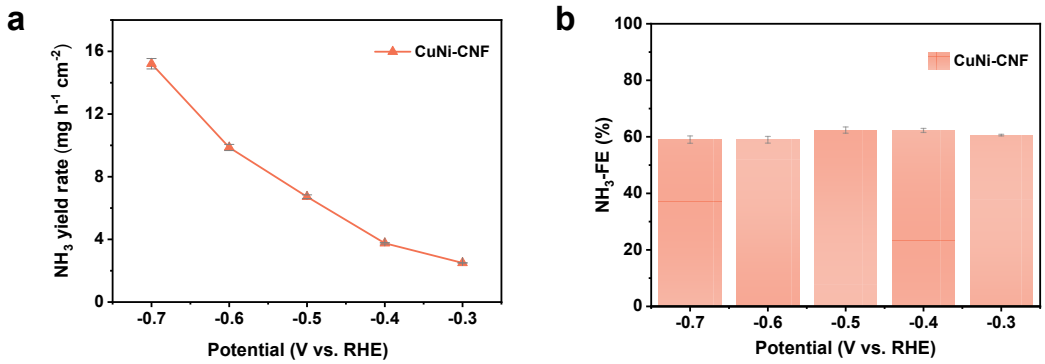

Fig. S9 a) The products formation rate of CuNi-CNF catalyst measured after 1 hour of chronoamperometry at different potential. b) Faraday efficiency of CuNi-CNF catalyst measured after 1 hour of chronoamperometry at different potential.

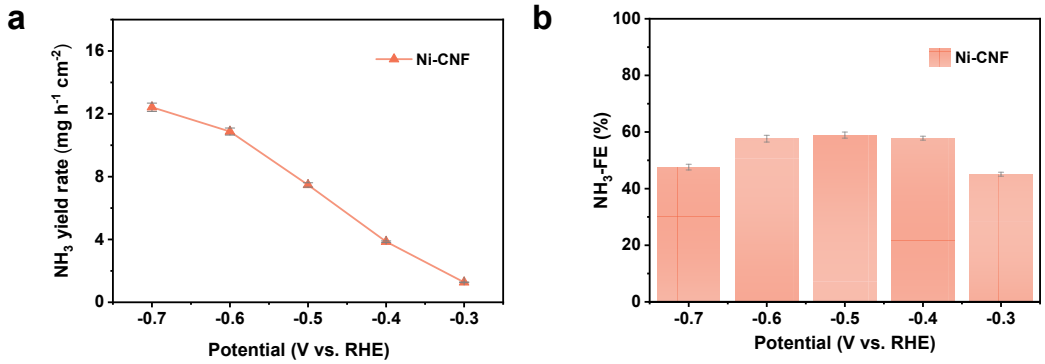

Fig. S10 a) The products formation rate of Ni-CNF catalyst measured after 1 hour of chronoamperometry at different potential. b) Faraday efficiency of Ni-CNF catalyst measured after 1 hour of chronoamperometry at different potential.

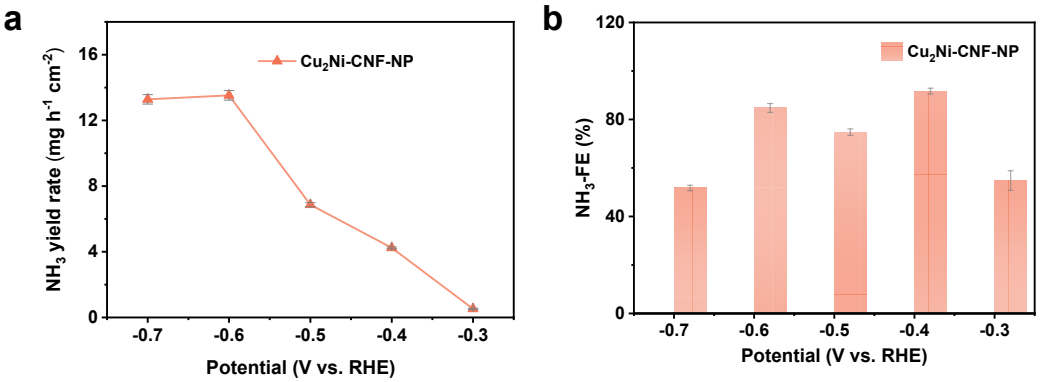

Fig. S11 a) The products formation rate of Cu_2Ni-CNF-NP catalyst measured after 1 hour of chronoamperometry at different potential. b) Faraday efficiency of Cu_2Ni-CNF-NP catalyst measured after 1 hour of chronoamperometry at different potential.

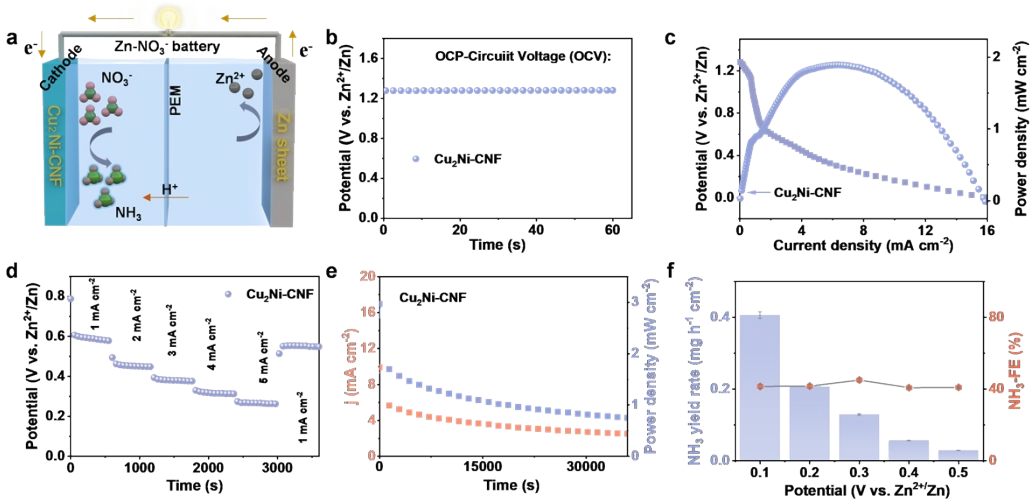

Fig. S12 Electrochemical performance of the Zn-NO_3^- battery based on the Cu_2Ni-CNF cathode. a) Schematic illustration of the Zn- NO_3^- battery. b) OCV of the battery. c) Discharge polarization and power density curves. d) Galvanostatic discharge profiles at different current densities. e) Long-term discharge curve. f) NH_3 yield rate and Faradai c efficiency of NH_3 formation during battery discharge.

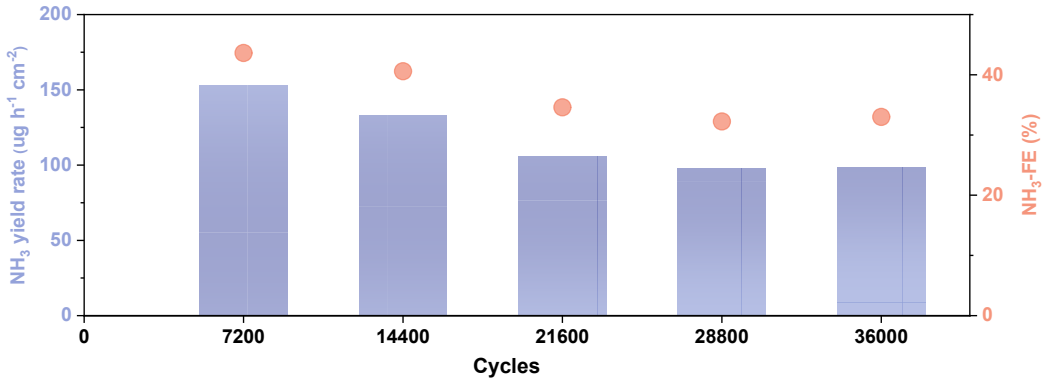

Fig. S13 The long-term cycle stability of the Zn-NO_3^- battery.

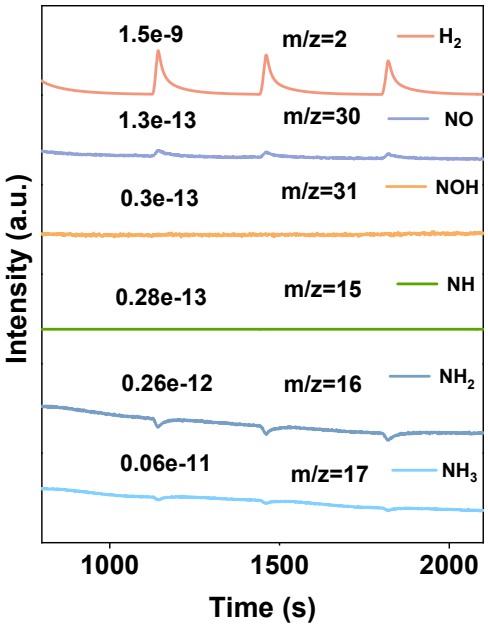

Fig. S14 In situ DEMS measurement of Ni-CNF for NO_3RR.

Table S1 Comparison of the electrocatalytic NO_3RR performances of Cu_2Ni-CNF with other reported electrocatalysts.

Catalyst	Electrolyte	Potential V (vs. RHE)	FE (%)	Yield rate (mg cm^{-2} h^{-1})	NH_3-Current Density (mA cm^{-2})	Ref.
Cu_2Ni-CNF	1.0 M KOH	-0.5	96.38	8.6876	118	This work
FL-Ag/HEA/CNFs	1.0 M KOH	-0.23	90.5	3.519	/	S1
Fe-NBC	0.5 M K_2SO_4	-0.64	75.3	1.3362	/	S2
$Pd_{63}Cu_{37}$ MSs	0.1 M KOH	-0.25	85.0	0.306	/	S3
Cu-CoP	0.1M K_2SO_4	-1	85.01	7.65	/	S4
Pd cuboct a	0.1 M NaOH	-0.2	35	0.3068	/	S5
Co_3O_4@CuO-0.4	/	-0.6V	/	/	2500	S6
CuPc/FeNC	1 M KOH	-0.57	~100%	/	273	S7
CuNi	1 M KOH	-0.2	95.33%	48.8 mg h^{-1} cm^{-2}	-129	S8
NF/Ni_3NCu	/	-0.3	98.7%	/	/	S9
Cu-TCPP/Cu_2O/CF	0.1 M Na_2SO_4	-1	90.22%	/	/	S10
CuNi NPs /CF	1 M NaOH	-0.48	97.03%	94.57 mmol h^{-1} cm^{-2}	1164	S11

Table S2 ICP-OES results of Cu_2Ni-CN catalyst.

Element	Atomic ratio (%)	Elemental content (%)
Cu	66.77	14.5
Ni	33.23	7.22

References

[S1] J. Hao, T. Wang, R. Yu, J. Cai, G. Gao, Z. Zhuang, Q. Kang, S. Lu, Z. Liu, J. Wu, G. Wu, M. Du, D. Wang and H. Zhu, Nature Communications, 2024, 15, 9020.

[S2] S.-F. Jiang, Z.-Y. Hu, S. Chen, H.-C. Hao and H. Jiang, Journal of Environmental Chemical Engineering, 2024, 12, 111915.

[S3] L. Sun, H. Yao, F. Jia, Y. Wang and B. Liu, Advanced Energy Materials, 2023, 13, 2302274.

[S4] W. Yang, Z. Chang, X. Yu, P. Wu, R. Shen, L. Wang, X. Cui and J. Shi, Advanced Science, 2025, 12, 2416386.

[S5] J. Lim, C.-Y. Liu, J. Park, Y.-H. Liu, T. P. Senftle, S. W. Lee and M. C. Hatzell, ACS Catalysis, 2021, 11, 7568-7577.

[S6] H. Xu, Y. Yang, A. Han, C. Yao, H. Zhang, Y. Luo, Z. Fu, Y. Lu, G. Liu, F. Li and D. Zhao, Angewandte Chemie International Edition, 2025, 64, e202510450.

[S7] Y. Wang, S. Wang, Y. Fu, J. Sang, Y. Zang, P. Wei, H. Li, G. Wang and X. Bao, Chinese Journal of Catalysis, 2024, 56, 104-113.

[S8] Y. Li, B. Long, Y. Cui, W. Li, D. He, Z. Ke and X. Xiao, ACS Nano, 2025, 19, 25939-25950.

[S9] X. Ouyang, W. Qiao, Y. Yang, B. Xi, Y. Yu, Y. Wu, J. Fang, P. Li and S. Xiong, Angewandte Chemie International Edition, 2025, 64, e202422585.

[S10] Y. Dong, C. Zhao, Y. Li, Y. Guo, X. Liu, W. Liu, R. Souiki, S. Ding and B. Guo, ACS Applied Energy Materials, 2025, 8, 9038-9048.

[S11] W. Yu, J. Yu, M. Huang, Y. Wang, Y. Wang, J. Li, H. Liu and W. Zhou, Energy & Environmental Science, 2023, 16, 2991-3001.